Advanced NO_2 Gas Sensor Fabrication through UV Laser-Induced Selective Reduction Laser Sintering

Wang, Shaogang; Zong, Qihang; Yang, Huiru; Huang, Qianming; Ye, Huaiyu; French, Paddy

DOI
10.1109/NEMS60219.2024.10639835

Publication date
2024

Document Version
Final published version

Published in
2024 IEEE 19th International Conference on Nano/Micro Engineered and Molecular Systems, NEMS 2024

Advanced NO_2 Gas Sensor Fabrication through UV Laser-Induced Selective Reduction Laser Sintering

Shaogang Wang [†‡], Qihang Zong[‡], Huiru Yang[‡], Qianming Huang[‡], Huaiyu Ye[†‡], Paddy French[†*]

[†]Email: s.wang-10@tudelft.nl yehy@sustech.edu.cn p.j.french@tudelft.nl

[†]The Faculty of EEMCS, Delft University of Technology, Delft, Netherlands

[‡]The School of Microelectronic, Southern University of Science and Technology, Shenzhen, China

2024 IEEE 19th International Conference on Nano/Micro Engineered and Molecular Systems (NEMS) | 979-8-3503-5983-1/24/$31.00 ©2024 IEEE | DOI: 10.1109/NEMS60219.2024.10639835

***Abstract*—This study introduces an innovative approach for fabricating flexible nitrogen dioxide (NO_2) gas sensors based on In2O3 nanoparticles (NPs) using selective reduction laser sintering (SRLS) technology. The SRLS technology enables specific chemical reduction reactions during the sintering process, achieving fabrication and control of oxygen vacancy defects and the porous structure in the In_2O_3 sintering region. The sensor exhibits exceptionally high sensitivity, fast response/recovery times, and superior selectivity for NO_2 gas detection, particularly at room temperature. Compared with traditional NO_2 gas sensor fabrication methods, this technology not only provides a potential way to fabricate high-performance NO_2 gas sensors but also further expands the application potential of laser direct writing (LDW) technology in the fields of advanced materials and sensor fabrication.**

***Keywords*—Flexible gas sensor, NO_2 detection, Indium oxide nanoparticles, Selective reduction laser sintering.**

I. Introduction

The rapid progress of wearable technology has extensively promoted the innovation of advanced flexible sensors, enabling them to become an essential tool for personal health monitoring, assessment, and intervention [1]. Nitrogen dioxide (NO_2), a byproduct of fossil fuel combustion, is critical to monitoring the environment and public health. NO_2 gas is not only destructive in terms of acid rain, photochemical smog, and thinning of the ozone layer but may also pose a threat to human health when its concentration exceeds 3 ppm [2]. Therefore, it is vital to develop sensors that can quickly detect NO_2. Indium oxide (In_2O_3) based sensors have attracted attention for their excellent sensitivity and fast response, and performance enhancement has been achieved through innovative approaches such as heterostructures, doping technology, and metal catalysis [3]. However, the limitations of these sensors in terms of selectivity, operating temperature, and humidity sensitivity remain challenges that need to be addressed [4]. Laser direct writing (LDW) technology, particularly selective laser sintering (SLS), offers a new solution to these challenges through its ability to process materials and devices with precision and customization.

In this study, we report a novel flexible gas sensor fabricated using selective reduction laser sintering (SRLS) technology, designed to detect NO_2 at room temperature. This technology achieves the selective reduction of PVP-coated In_2O_3 nanoparticles (NPs) by controlling the critical parameters of UV pulse laser, thereby achieving precise modification of materials and rapid fabrication of devices. Due to the synergistic effect of oxygen vacancy defects and porous structure in the sintering region, the sensor exhibits high sensitivity (442.24), fast response/recovery times (30/570 s), and superior selectivity to NO_2 gas at room temperature.

II. Results and Discussion

A. Mechanism of Selective Reduction Laser Sintering

Unlike traditional selective laser sintering (SLS), which directly irradiates laser light onto the material surface to achieve high-temperature solid phase conversion, selective reduction laser sintering (SRLS) achieves material sintering by finely regulating the temperature distribution along the edge of the laser scanning path. The flexible NO_2 gas sensor fabrication using this technology contains four primary steps, as shown in Fig. 1(a). First, the In_2O_3 NPs paste was uniformly coated on the PET (Polyethylene terephthalate) substrate using a combination of four-sided scraper and doctor blade method. Next, after the solvent was evaporated entirely at room temperature, the In_2O_3 layer was finely linearly laser-sintered using a computer-controlled ultraviolet (UV) laser system. Subsequently, the PET substrate was carefully cleaned with deionized water to remove the remaining unsintered In_2O_3 NPs paste. Finally, the silver electrodes for the sensor were printed on the PET substrate using screen printing technology.

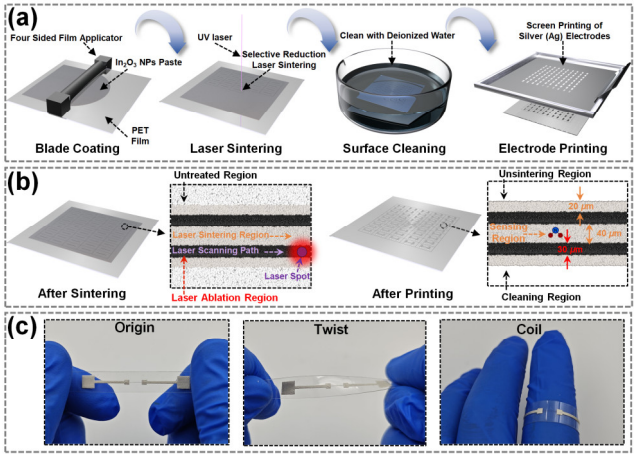

Fig. 1. (a) Schematic flow diagram of the flexible NO_2 gas sensor fabrication process. (b) Schematic diagrams of the overall and localized surface of In_2O_3 nanoparticles (NPs) in the laser sintering and laser ablation regions after the sintering and printing processes. (c) Comparison images of flexible gas sensors in different deformation states.

In the SRLS process, In_2O_3 NPs are not only the critical material of flexible gas sensors but also the primary coating that triggers photothermal effects. It is widely recognized that PET has a relatively low absorption coefficient for ultraviolet (UV) laser. Therefore, when the laser is irradiated vertically onto the PET film, most of the laser energy will pass through the PET without causing any apparent physical or chemical reaction to the PET [5]. However, when the PET surface is coated with In_2O_3 NPs, the In_2O_3 layer absorbs the UV laser energy and rapidly converts it into thermal energy.

This photothermal conversion action produces a significant photothermal effect on the PET surface, which is essential for achieving a precise sintering process. Under UV laser irradiation, the high laser energy density causes slight ablation of the PET substrate underneath the In_2O_3 layer. At the same time, the high-temperature gradient generated by this laser ablation region promotes the thermal sintering of In_2O_3 at the edges of the laser scanning path. As a result, the In_2O_3 NPs melt and aggregate, forming a unique laser sintering region. On the contrary, unsintered In_2O_3 NPs can be easily removed by cleaning with deionized water, as shown in Fig. 1(b). It is worth noting that the benefit from the fast laser scanning speed (10 mm/s) and small laser radius (6.5 μm), this technology significantly reduces the impact on the substrate compared to conventional high-temperature sintering and hot-press sintering processes. As a result, the SRLS technology can be easily realized even on 250 μm PET films, enabling the fabrication of gas sensors with a variety of patterns. The fabricated flexible gas sensor can maintain stable mechanical properties under various deformation states, such as finger twisting and curling, as shown in Fig. 1(c).

B. *Characterization of Oxygen Vacancy Defects*

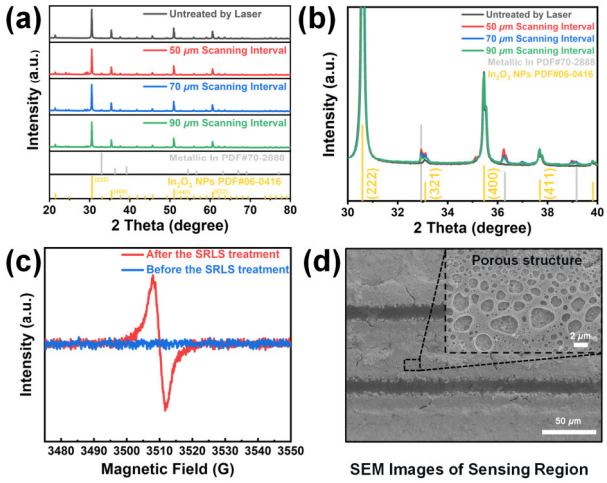

Fig. 2. (a) Overall and (b) localized X-ray diffraction (XRD) patterns of In_2O_3 NPs paste before and after the SRLS treatment at different scanning intervals. (c) Electron paramagnetic resonance (EPR) spectra of In_2O_3 NPs paste before and after the SRLS treatment. (d) Scanning electron microscope (SEM) images of the sensing region of the sensor.

To investigate the effect of different laser scanning intervals on the crystal structure and phase transformation of In_2O_3 NPs paste during the selective reduction laser sintering (SRLS) process, we characterized the untreated and 50 μm, 70 μm, and 90 μm scanning intervals of the samples by using X-ray diffraction (XRD) and analyzed their XRD patterns, as shown in Fig. 2(a). The XRD pattern of the In_2O_3 NPs untreated by the SRLS process predominantly indicates characteristic peaks of the In_2O_3 phase located at 30.6°, 35.5°, 51.0°, and 60.7°, corresponding to the (222), (400), (440), and (622) crystal planes (PDF#06-0416). However, the In_2O_3 NPs treated with the SRLS process at different scanning intervals, in addition to characterizing the peaks of In_2O_3, also exhibits XRD characteristic peaks of metallic indium, located at 32.9°, 36.3°, 39.2°, and 54.4°, respectively (PDF#70-2888). Comparing the overall intensity of the XRD peaks, it is evident that the transition from In_2O_3 to metallic indium is relatively slight.

Further, especially in the diffraction angle range of 30° to 40°, the intensity of the metallic indium characteristic peaks near the (321) and (400) crystal planes of In_2O_3 increases significantly as the laser scanning interval decreases, as shown in Fig. 2(b). Meanwhile, the XRD pattern reveals that as the average sintering temperature increases due to the reduction of the laser scanning interval, the XRD diffraction peak near the In_2O_3 (321) crystal plane moves to a higher 2θ diffraction angle [6, 7]. This transformation indicates a decrease in the lattice constant of In_2O_3, resulting in a more compact lattice structure. It also shows that the indium ions in In_2O_3 are reduced to lower valence states or even reduced to metallic indium, and implies the formation of oxygen vacancy defects [8].

Additionally, the electron spin resonance (EPR) results further demonstrate the significant signal at a g value of 2.0 for In_2O_3 nanoparticles after the SRLS treatment, as shown in Fig. 2(c). During the SRLS process, the reducing macromolecules generated by the decomposition of the main chain of PVP reduce In_2O_3 to metallic indium while forming oxygen vacancy defects. These oxygen vacancy defects trap the electrons, resulting in the formation of a distinct signal in the EPR spectrum. This result further proves the existence of oxygen vacancy defects after the SRLS treatment [9].

Fig. 2(d) shows the scanning electron microscope (SEM) images of the sensing region of the flexible gas sensor. Interestingly, the ablation of the PET substrate during the SRLS process results in sputtering at the edges of the sintering region, leading to the formation of a porous structure. This not only enhances the adhesion between the In_2O_3 NPs and the PET substrate in the sintering region but also increases the specific surface area of the sensing region to some extent. As a result, the In_2O_3 NPs sensing material with oxygen vacancy defects is able to capture more target gases, which in turn improves the sensitivity of the sensor.

C. *Performance of Flexible Gas Sensors*

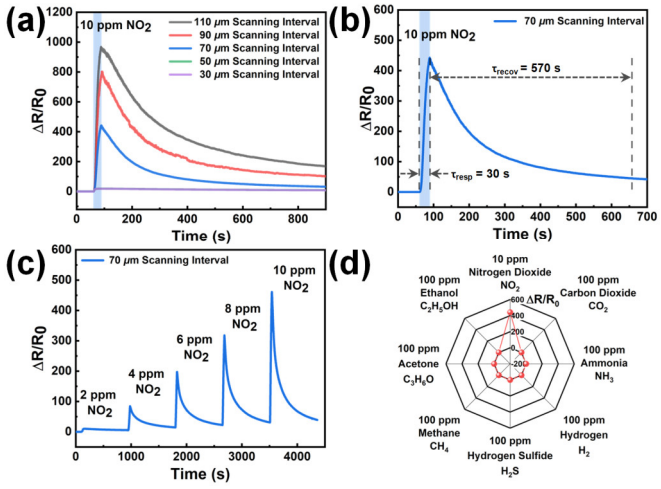

Fig. 3. (a) The response curves of the gas sensors based on In_2O_3 NPs for 10 ppm NO_2 at different scanning intervals. (b) The response curves of the gas sensors based on In_2O_3 NPs for 10 ppm NO_2 at different scanning intervals. (c) Dynamic response curve of the gas sensor to NO_2 from 2 to 10 ppm at room temperature. (d) Radar plot of gas sensor selectivity test for NO_2 relative to other interfering gases (C_2H_5OH, CO_2, C_3H_6O, NH_3, CH_4, and H_2S).

During the SRLS process, the difference in sintering temperature induced by the laser scanning interval is highly

critical to the performance of N-type chemoresistive gas sensors based on In_2O_3 NPs. To fully evaluate this effect, the sensor was exposed to a specific concentration of NO_2 gas at room temperature (25°C) for 30 seconds. The evaluation equation for the sensor sensitivity was defined as $S=\Delta R/R_a=(R_g-R_a)/R_a$ with a bias voltage of 1.0 V, where R_a and R_g represent the stabilized resistance values of the sensor in air and in the target gas environment, respectively. Response time (τ_{resp}) and recovery time (τ_{reco}) were determined by the time required for the sensor resistance value to reach a 90% change after exposure to NO_2 and upon subsequent re-exposure to air, respectively [10].

Test results show a rapid increase in resistance when the sensor is placed in 10 ppm NO_2 gas, followed by a gradual fall back in the air environment, as shown in Fig. 3(a). It is noteworthy that the average sintering temperature of the In_2O_3 NPs sensing region decreases as the laser scanning interval increases. Nevertheless, the sensor sensitivity to NO_2 gas shows an increasing trend, reaching values of 18.27, 19.69, 442.24, 802.16, and 967.62, respectively. In fact, the stabilized resistance value (R_a) of the sensor in the air shows an increasing trend as the laser scanning interval increases. Although intuitively, an increase in R_a would seem to decrease sensitivity (due to an increase in the denominator), sensor sensitivity actually shows an upward trend as the laser scan interval expands. This indicates that the creation of oxygen vacancy defects plays a decisive role in enhancing the sensitivity of the sensor. In other words, even though the increase in initial sensor resistance may not be favorable to the improvement of sensitivity, the increase in oxygen vacancy defects still plays a crucial role in improving the sensitivity of the device [11]. In detail, the increase in oxygen vacancy defects provides both more adsorption sites for target gas molecules and increases the number of free electrons in the conduction band. This further reduces the difficulty of electron capture by the target gas molecules. As a result, the resistance of the sensor increases significantly during operation, reflecting its sensitive response to the NO_2 gas.

However, the increase in the density of oxygen vacancy defects, while enhancing the adsorption of the NO_2 gas on the sensor surface, also affects the rapid recovery capability of the sensor. Furthermore, the increase in the laser scanning interval led to a decrease in the average sintering temperature, which in turn weakened the adhesion between the In_2O_3 nanoparticles and the PET substrate. As a result, the quality of the sintered structure decreases, which poses a challenge to the stability and reliability of the sensor. In order to strike a balance between performance and stability, subsequent studies will focus on the selection of In_2O_3 NPs based sensors with a scanning interval of 70 μm for performance evaluation. The fast response and recovery times of this sensor for 10 ppm NO_2 at room temperature are 30 and 660 s, respectively, as shown in Fig. 3(b).

In addition, the response of the sensor increased from 9.8 to 460.9 when the NO_2 gas concentration increased from 2 ppm to 10 ppm, demonstrating its excellent dynamic response and recovery capability, as shown in Fig. 3(c). Significantly, the sensor responds much better to 10 ppm NO_2 than to 100 ppm concentrations of interfering gases, including C_2H_5OH, CO_2, C_3H_6O, NH_3, CH_4, and H_2S, demonstrating its excellent selectivity, as shown in Fig.3 (d).

As a result, gas sensors fabricated using SRLS technology and based on In_2O_3 NPs exhibit high sensitivity, fast response/recovery, and excellent selectivity. This method has obvious advantages over the conventional fabrication method of In_2O_3-based gas sensors.

D. Performance of Flexible Gas Sensors

The primary sensing mechanism of the NO_2 gas sensor based on In_2O_3 NPs fabricated using the SRLS technology at room temperature mainly relies on the conductivity changes triggered by the adsorption and desorption of gas molecules on the surface of the sensing region [12]. In particular, oxygen vacancy defects on the In_2O_3 surface play a crucial role in this process. They promote the transition of electrons from the valence band to the conduction band, which significantly increases the concentration of free electrons in the conduction band, leading to a decrease in the sensor resistance.

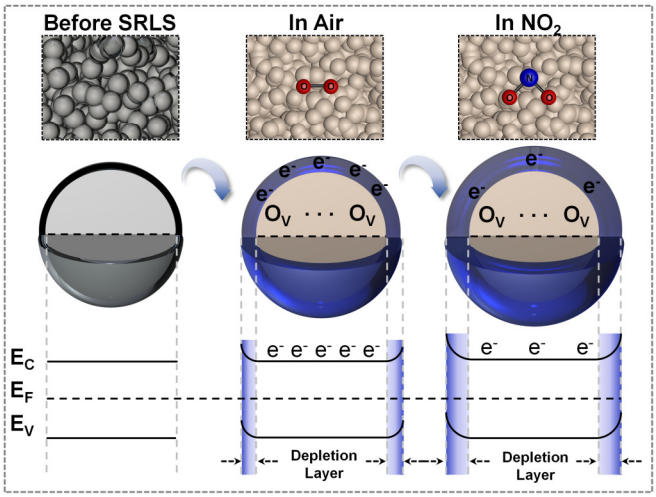

Fig. 4. The schematic diagram of the NO_2 surface sensing mechanism of a flexible gas sensor based on In_2O_3 NPs fabricated using the SRLS technology. (E_C: conduction band; E_F: fermi energy; E_V: valence band).

In the air atmosphere, oxygen molecules (O_2) are adsorbed to the surface of In_2O_3 NPs and capture free electrons from the conduction band of In_2O_3 to from $O_{2(ads)}^-$ ions with higher chemical activity [13], as detailed in the reaction equations (1) and (2) [14]. Meanwhile, this process reduces the carrier concentration on the surface of the In_2O_3, causing the energy band to bend upward and forming a surface electron depletion layer, as shown in Fig. 4.

$$O_{2(gas)} \leftrightarrow O_{2(ads)} \quad (1)$$

$$O_{2(ads)} + e^- \rightarrow O_{2(ads)}^- \quad (2)$$

When the sensor is exposed to the NO_2 gas environment, the NO_2 molecules directly interact with the electrons in the conduction band of the In_2O_3 to form NO_2^- ions due to their high electron affinity [13]. In addition, the NO_2 molecules can also interact directly with already existing $O_{2(ads)}^-$ ions to form NO_3^- ions, as detailed in the reaction equations (3) and (4) [15]. Meanwhile, this process further increases the depth of the electron depletion layer on the surface of the In_2O_3, resulting in a further upward bending of the energy band and a significant increase in the resistance of the material.

$$NO_{2(ads)} + e^- \rightarrow NO_{2(ads)}^- \quad (3)$$

$$O_{2(ads)}^- + 2NO_{2(ads)} \rightarrow 2NO_{3(ads)}^- \quad (4)$$

Both of these effects lead to a reduction in the conduction band electrons of In_2O_3 NPs, which in turn increases the thickness of the electron depletion layer and the potential barrier. However, due to the strong oxidizing nature of NO_2, it dominates at room temperature, significantly increasing the sensor resistance. The subsequent desorption process works in reverse and further reduces the resistance of the sensor. Therefore, the excellent performance of the NO_2 gas sensor based on In_2O_3 NPs fabricated by SRLS technology at room temperature is mainly attributed to the synergistic effect of oxygen vacancy defects and surface porous structure.

III. Conclusion

In summary, we have successfully demonstrated a new method of fabricating flexible gas sensors using selective reduction laser sintering (SRLS) technology to detect nitrogen dioxide (NO_2) at room temperature. The SRLS technology utilizes a UV-pulsed laser that enables the selective reduction of PVP-coated In_2O_3 NPs on a PET substrate, resulting in the fabrication of oxygen vacancy defects and porous structures in the sensing region. The sensors designed by this technology exhibit excellent performance, such as high sensitivity (442.24), fast response/recovery time (30/570 s), and high selectivity for NO_2. This technology provides a new solution to the challenges of In_2O_3-based gas sensors in terms of selectivity and operating temperature and expands the potential of laser direct writing (LDW) technology for advanced materials and sensor fabrication applications.

Acknowledgment

We want to express our deepest gratitude to Shenzhen Yixin Information Technology Co., Ltd. Their unwavering support, technical expertise, and dedication played an integral role in the success of our project.

References

[1] Y. Gao, L. Yu, J. C. Yeo, and C. T. Lim, "Flexible hybrid sensors for health monitoring: materials and mechanisms to render wearability," Advanced Materials, vol. 32, no. 15, p. 1902133, 2020.

[2] K. Wetchakun et al., "Semiconducting metal oxides as sensors for environmentally hazardous gases," Sensors and Actuators B: Chemical, vol. 160, no. 1, pp. 580-591, 2011.

[3] K. K. Pawar et al., "Hollow In_2O_3 microcubes for sensitive and selective detection of NO_2 gas," Journal of Alloys and Compounds, vol. 806, pp. 726-736, 2019.

[4] S. M. Majhi, S. Navale, A. Mirzaei, H. W. Kim, and S. S. Kim, "Strategies to Boost Chemiresistive Sensing Performance of In_2O_3-based Gas Sensors: An Overview," Inorganic Chemistry Frontiers, 2023.

[5] S. S. Ham and H. Lee, "Surface Characteristics of Polymers with Different Absorbance after UV Picosecond Pulsed Laser Processing Using Various Repetition Rates," Polymers, vol. 12, no. 9, p. 2018, 2020.

[6] D. Marrocchelli, S. R. Bishop, H. L. Tuller, and B. Yildiz, "Understanding chemical expansion in non-stoichiometric oxides: ceria and zirconia case studies," Advanced Functional Materials, vol. 22, no. 9, pp. 1958-1965, 2012.

[7] K. Bhattacharyya et al., "The formation and effect of O-vacancies in doped TiO_2," New Journal of Chemistry, vol. 44, no. 20, pp. 8559-8571, 2020.

[8] Q. Hou et al., "Defect formation in In_2O_3 and SnO_2: A new atomistic approach based on accurate lattice energies," Journal of Materials Chemistry C, vol. 6, no. 45, pp. 12386-12395, 2018.

[9] M. Meng et al., "Boosted photoelectrochemical performance of In_2O_3 nanowires via modulating oxygen vacancies on crystal facets," Journal of Alloys and Compounds, vol. 845, p. 156311, 2020.

[10] N. Joshi, T. Hayasaka, Y. Liu, H. Liu, O. N. Oliveira, and L. Lin, "A review on chemiresistive room temperature gas sensors based on metal oxide nanostructures, graphene and 2D transition metal dichalcogenides," Microchimica Acta, vol. 185, pp. 1-16, 2018.

[11] J. Gan et al., "Oxygen vacancies promoting photoelectrochemical performance of In_2O_3 nanocubes," Scientific reports, vol. 3, no. 1, p. 1021, 2013.

[12] N. Wang et al., "Rapid and accurate detection of highly toxic NO_2 gas based on catkins biomass-derived porous In_2O_3 microtubes at low temperature," Sensors and Actuators B: Chemical, vol. 361, p. 131692, 2022.

[13] Z. Cheng, L. Song, X. Ren, Q. Zheng, and J. Xu, "Novel lotus root slice-like self-assembled In_2O_3 microspheres: synthesis and NO_2-sensing properties," Sensors and Actuators B: Chemical, vol. 176, pp. 258-263, 2013.

[14] Y. Shen et al., "In-situ growth of mesoporous In_2O_3 nanorod arrays on a porous ceramic substrate for ppb-level NO_2 detection at room temperature," Applied Surface Science, vol. 498, p. 143873, 2019.

[15] Y.-K. Lv, Y.-Y. Li, R.-H. Zhou, Y.-P. Pan, H.-C. Yao, and Z.-J. Li, "N-doped graphene quantum dot-decorated three-dimensional ordered macroporous In_2O_3 for NO_2 sensing at low temperatures," ACS Applied Materials & Interfaces, vol. 12, no. 30, pp. 34245-34253, 2020.